Cement and Concrete Research 42 (2012) 1032–1041

Contents lists available at SciVerse ScienceDirect

Cement and Concrete Research

journal homepage: http://ees.elsevier.com/CEMCON/default.asp

Hydration of C_3A–gypsum systems

Alexandra Quennoz *, Karen L. Scrivener

Laboratory of Construction Materials, École Polytechnique Fédérale de Lausanne (EPFL), Station 12, CH-1015 Lausanne, Switzerland

ARTICLE INFO

Article history:
Received 28 November 2011
Accepted 16 April 2012

Keywords:
Ca3Al2O6 (D)
Gypsum
Calorimetry (A)
X-ray diffraction (B)
Microstructure (B)

ABSTRACT

Hydration of C_3A–gypsum systems with different gypsum additions was investigated in terms of the phase assemblage, kinetics and microstructural development. The second stage of the reaction, which begins after the depletion of gypsum, was of particular interest. From in-situ X-ray diffraction results, it was seen that the dissolution of ettringite and C_3A to form monosulfoaluminate and/or hydroxy-AFm phases is a rapid reaction that occurs right after the depletion of gypsum. The observation of the calorimetric curves obtained for the different gypsum additions leads us to the conclusion that the mechanism controlling the hydration rate during this period is the nucleation and growth of the AFm phases. The microstructural study showed that the formation of AFm phases occurs in the space between the C_3A grains but also within the boundaries of the original C_3A grains. Hydrogarnet was observed growing as a shell around the C_3A grains.

1. Introduction

Tricalcium aluminate (C_3A) is one of the main constituents of Portland cement. Even though it is typically less than 10% of the total composition, its uncontrolled reaction with water can lead to rapid setting, called flash set. Gypsum is added to regulate this reaction and preserves the workability of the cement paste during the first hours. Understanding the basics of the C_3A–gypsum reaction is therefore crucial for the comprehension of the early hydration of cement. Furthermore, an important route for the development of new cementitious materials is the partial replacement of clinker with supplementary cementitious materials; these can affect the reaction of C_3A and the sulfate balance. The comprehension of the mechanism of reaction of C_3A in the presence of calcium sulfate is therefore of major interest.

The general pattern of C_3A hydration alone and in the presence of gypsum is well known. When the hydration of C_3A occurs alone, C_3A reacts quickly with water to form platelets of calcium aluminate hydrates (Eq. (1)):

$$2C_3A + 21H \rightarrow C_4AH_{13} + C_2AH_8. \quad (1)$$

Depending on the water content the AFm phase C_4AH_{13} may contain more water in the interlayer and exists as C_4AH_{19}. The hydrate assemblage on the right hand side of Eq. (1) is metastable with respect to cubic hydrogarnet (C_3AH_6) to which it finally converts.

In the presence of calcium sulfate, the reaction can be divided in two stages. The first stage occurs when gypsum is present in the system and ettringite (AFt phase), is formed (Eq. (2)):

$$C_3A + 3C\$H_2 + 26H \rightarrow C_6A\$_3H_{32}. \quad (2)$$

The second stage of the reaction starts when the supply of sulfate ions runs out. There is a surge in C_3A dissolution and the remaining C_3A reacts with ettringite and water to form monosulfoaluminate (Eq. (3)) (and hydroxy-AFm (Eq. (1)) depending on the initial gypsum content):

$$2C_3A + C_6A\$_3H_{32} + 4H \rightarrow 3C_4A\$H_{12}. \quad (3)$$

Most previous studies have focused on the mechanisms controlling the first stage of the C_3A–gypsum reaction, to explain why calcium sulfate slows down the reaction of C_3A. Two main hypotheses have been discussed in the past decades. On one hand, it is claimed that the reaction is limited by a layer of hydration products. This layer is usually purported to be ettringite [1,2], but AFm has also been claimed as the "blocking" hydrate [3–8]. On the other hand, it has been proposed that the adsorption of calcium and sulfate ions on active dissolution sites of C_3A slows down the reaction rate [9–12]. Scrivener and Pratt [8] pointed out that the morphology of ettringite is unlikely to provide a substantial barrier to ion transport and Minard et al. [10] clearly showed that the calcium aluminate phase that can be observed on C_3A surface at the beginning of the reaction is an AFm hydrate. However, this hydrate also forms in pure C_3A where the reaction is not slowed down and does not form in the presence of hemihydrate where it is slowed [12]. Therefore, such a layer cannot be at the origin of the slowdown of the reaction.

* Corresponding author. Tel.: +41 21 635 22 17.
E-mail address: alexandra.quennoz@a3.epfl.ch (A. Quennoz).

0008-8846/$ – see front matter © 2012 Elsevier Ltd. All rights reserved.
doi:10.1016/j.cemconres.2012.04.005

Moreover, Minard et al. observed a constant hydration rate of C_3A during the first stage of the reaction (when the effects of particle size are accounted for) which is not compatible with an inhibiting layer which should thicken and further slow the reaction with time. The evidence now available firmly supports the second theory of inhibition by absorption of sulfate ions at reactive sites, although Pourchet et al. claim that the precipitation of ettringite may also play a role in controlling the composition of the solution [12].

The reactions that occur after the depletion of gypsum as well as the later ages have been less extensively studied and many points, such as the mechanisms controlling the hydration rate or the microstructural development are still unclear. The new contribution of this paper is therefore mainly in this second stage. The reaction kinetics was also investigated at different temperatures. Both stages of the reaction obey an Arrhenius relationship and the activation energies were calculated. The phase assemblages formed as a function of the gypsum content were followed by in-situ XRD during the first days of reaction to elucidate the kinetics of the evolution of the phases after gypsum depletion. The influence of several parameters (specific surface area of C_3A and w/s ratio) on the kinetics during the second stage of the reaction was studied in order to identify the mechanisms controlling the hydration rate. Finally, the microstructural development of C_3A–gypsum systems was investigated.

2. Materials and methods

2.1. C_3A synthesis

C_3A was synthesized by sintering compacted powders of calcium carbonate and alumina at 1400 °C for 5 h preceded by a plateau of 8 h at 1000 °C to guarantee complete decarbonation of the calcium carbonate. The pellets were fired twice with an intermediate grinding to ensure homogeneity and complete reaction of the reactants. Finally, the pellets were ground and sieved and particles <80 μm were selected. The purity of the C_3A was checked by XRD. The quantitative analysis showed traces of free lime (1 to 2% depending on the batch). Different batches of C_3A were used for this study (A, B and C). We consider as a "batch" powders synthesized in the same conditions and homogenized before sieving. Even though great care was taken to synthesize all the C_3A batches in the same way, different particles size distributions and consequently different reaction rates were observed. The kinetics results obtained from the different batches can therefore not be directly compared and are presented separately. However some trends characteristics of the general C_3A–gypsum system can be observed. The particles size distributions (PSD) of the different batches of C_3A are presented in Fig. 1a). An investigation was also made of C_3A systems with very different particles size distributions. For this study the C_3A was sieved into two different PSD's; one called coarse (Dv 50 = 7 μm) and one fine (Dv 50 = 0.7 μm) as presented in Fig. 1b).

2.2. C_3A–gypsum sample preparation

Gypsum (PSD also shown in Fig. 1a)) from Merck was added to the ground C_3A. Gypsum additions between 7% of the C_3A up to 40% were studied. The powders were dry mixed in a *Turbula* shaker–mixer for 5 h and then gently co-ground for 5 min by hand in a mortar. C_3A–gypsum pastes were prepared at room temperature with a vertical mixer *IKA Labortechnik RW20.n*. Deionized water corresponding to a w/s ratio of 1 was added to the powder and mixed at 500 rpm during 2 min. A summary of the samples prepared for this study and the experiments carried out is presented in Table 1.

2.3. Calorimetry

The hydration of C_3A–gypsum pastes was followed by calorimetry at 20 °C in an isothermal calorimeter: *TAM Air* from *Thermometric*.

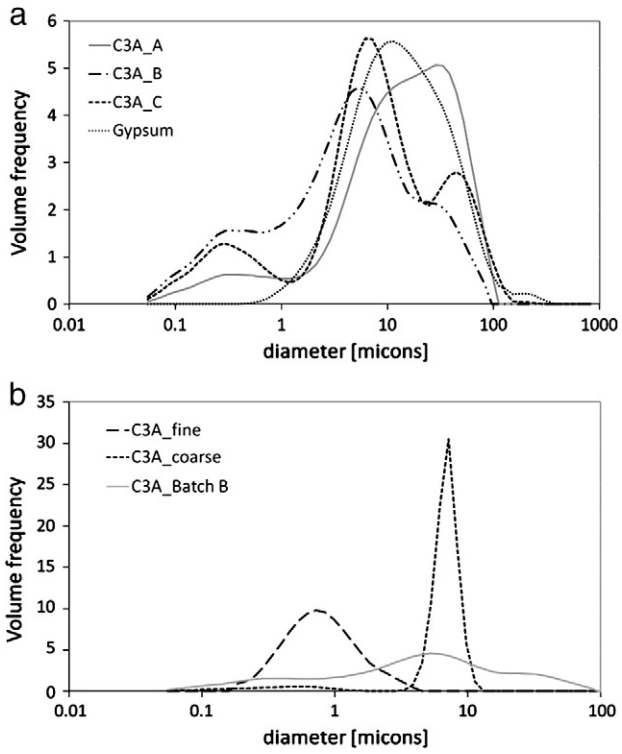

Fig. 1. a) Particles size distributions of the different batches of C_3A and gypsum. Particles from Batch A are slightly larger and therefore the specific surface area is smaller. b) Fine and coarse particles size distributions compared to a standard one (Batch B).

Pastes were mixed outside the calorimeter and the samples were introduced into the calorimeter as soon as possible (<5 min) after mixing. The reactions were studied at 20, 26 and 30 °C to determine the activation energy. The activation energies (Ea) for the different stages of the reaction were calculated with a method adapted from the Maturity method (e.g. [13]) that consists of calculating the

Table 1
Summary of the C_3A–gypsum samples and experiments carried out.

Samples\ experiments	Phase assemblage (XRD)	Microstructure (SEM)	Kinetics (calorimetry)
C3A_7%G (Batch A)			@20 °C
C3A_12%G (Batch A)			@20 °C different w/c
C3A_20%G (Batch A)			@20 °C
C3A_27%G (Batch A)			@20 °C
C3A_10%G (Batch B)	In-situ at early ages @26 °C + slices at later ages	1d, 3d, 7d, 28d	@20, 26, 30 °C
C3A_20%G (Batch B)	In-situ at early ages @26 °C + slices at later ages	3d, 7d, 28d	@20, 26, 30 °C
C3A_35%G (Batch B)	In-situ at early ages @26 °C + slices at later ages	3d, 7d, 28d	@20, 26, 30 °C
C3A_10%G (Batch C)			@20 °C
C3A_30%G (Batch C)			@20 °C
C3A_40%G (Batch C)			@20 °C
C3A_20%G (Batch D)		Evolution up to 35 h	
Fine 10%G, 20%G, 35%G			@20 °C
Coarse 10%G, 20%G			@20 °C

equivalent time factor necessary to superpose the calorimetry curves obtained at different temperatures. For the first stage of the reaction, the corresponding part of the cumulative heat evolution curves were mathematically superposed using the formula:

$$t_{eq} = \alpha \cdot t. \quad (4)$$

Where α is the age conversion factor needed to superpose the cumulative curves as shown in Fig. 2a). To determine the activation energy for the second stage of reaction the differential calorimetric curves were used and a similar method was used to superpose the slopes of the calorimetric peaks:

$$t_{eq} = \alpha \cdot (t + \beta). \quad (5)$$

Where α is the age conversion factor needed to superpose the slopes of the calorimetric peaks as shown in Fig. 2b) and β is a shift factor to align the start of the peak to help the determination of the age conversion factor. This β factor was not taken into account for the calculation of the activation energy.

The activation energies were then calculated with the following Eq. (6) where T_{ref} is 293 K:

$$E_a = \frac{\ln(\alpha) \cdot R}{\frac{1}{T} - \frac{1}{T_{ref}}}. \quad (6)$$

2.4. X-ray diffraction (XRD)

X-ray diffraction (XRD) patterns were collected with a *PANalytical X'Pert Pro MPD* diffractometer (*X'Celerator* detector) in a θ–θ configuration with a CuKα radiation (λ = 1.54 Å), a divergence slit size 0.5° and a rotating sample stage. To follow the evolution of the phase assemblage at early ages, in-situ XRD measurements were carried out. The same sample of fresh paste was measured continuously during the first 2 days of hydration. To avoid extensive loss of water and contact with CO_2 during hydration, a protective film (*kapton film HN50 form Maagtechnic*) was used to cover the cement paste. This technique has several advantages for studying hydration: patterns of a good resolution can be obtained with realistic sampling rate; and the use of wet samples instead of dry slices is particularly useful in the case of study of the aluminate hydrates such as ettringite and AFm as these hydrates are deteriorated by the usual drying techniques (e.g. [14]). Moreover the C_3A–gypsum samples, that are very sensitive to carbonation, are well protected from reaction with CO_2 with the use of the kapton film. However it is not possible to calculate absolute amounts of phases due to the contribution of the kapton film and the water in the sample; instead to plot the evolution of each phase, all the collected scans were plotted in a tridimensional plot (x = time, y = angles, z = counts), the background was calculated and removed, finally a peak representative of the phase was isolated and the evolution of this phase was calculated from the peak areas at different times, normalized to the maximum of this peak. With this technique it was possible to follow semi quantitatively the phase assemblage during the first hours of hydration and compare it to the calorimetric heat evolution profile. To ensure the comparability of the results the same original paste was separated in two parts after mixing: one part for the XRD measurements and the other for the calorimetry. The temperature in the XRD chamber was quite high but stable at 26 °C. The calorimetric measurements were therefore carried out at the same temperature (26 °C). However, a delay of the exothermic peak compare to the reactions measured by XRD was still observed. This delay was observed for all three samples studied. It is thought that this acceleration of the reaction measured by XRD may be due to an increase of the temperature in the vicinity of the sample in the XRD chamber probably caused by the heat developed by the sample during hydration. Therefore, both the measured calorimeter curve (plain curve) and the presumed calorimetric curve of the XRD samples (dot curve) are presented in Fig. 5. Using the activation energy calculated, the effective temperature of the sample in the XRD chamber was estimated to 28.5 °C instead of 26 °C.

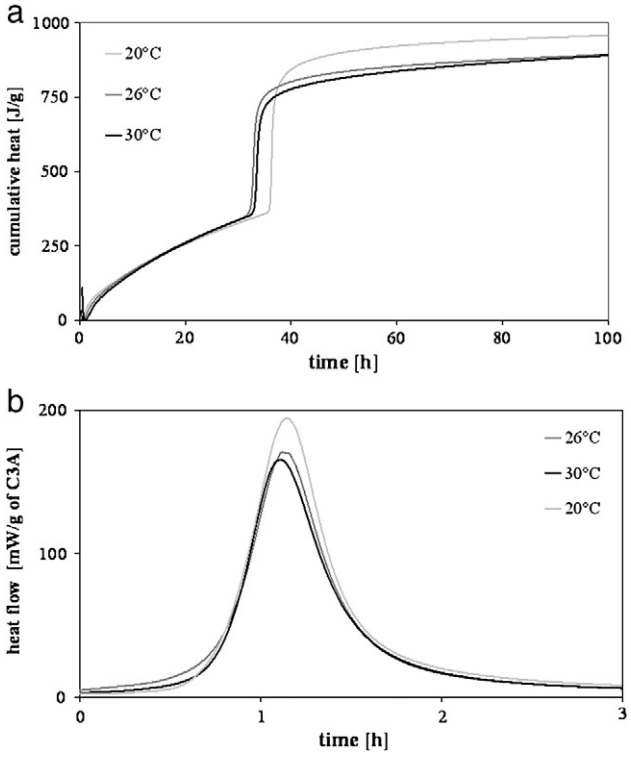

Fig. 2. Examples of superposition of calorimetry curves in order to determine the activation energy using the time equivalent method. a) For the first stage of the reaction. b) For the second stage.

For the study of the phase assemblage at later ages, pastes were prepared and hydrated in sealed containers. At defined times, a cylinder of set cement paste was cut into slices for XRD measurements. Although great care was taken to refill the sample container with N_2 after opening, some carbonation of these very sensitive samples could not be totally avoided.

2.5. Scanning electron microscopy (SEM)

In this study a *FEI quanta 200* SEM microscope with an accelerating voltage of 15 kV and a *Bruker AXS XFlash Detector* for energy dispersive X-ray analyses were used. For microscopy, pastes were cast into small plastic containers (10 mm of diameter and 25 mm height) and stored for hydration at controlled temperature. The hydration was stopped by freeze drying. The sample (with its container) was immersed in liquid nitrogen (−196 °C) for about 15 min. Due to the small size of the sample the pore water is almost instantly frozen. The frozen water was then removed by sublimation in a *Telstar Cryodos* freeze-dryer. Once dried, the samples were prepared for BSE–SEM observation by epoxy-impregnation (*EPOTEK-301*) and polished with a diamond powder down to 1 μm.

3. Results and discussion

3.1. Kinetics analysis of the first stage of the reaction (in the presence of gypsum)

Fig. 3 shows the heat evolution curves for two series of experiments. It can be observed that the exothermic peak characterizing

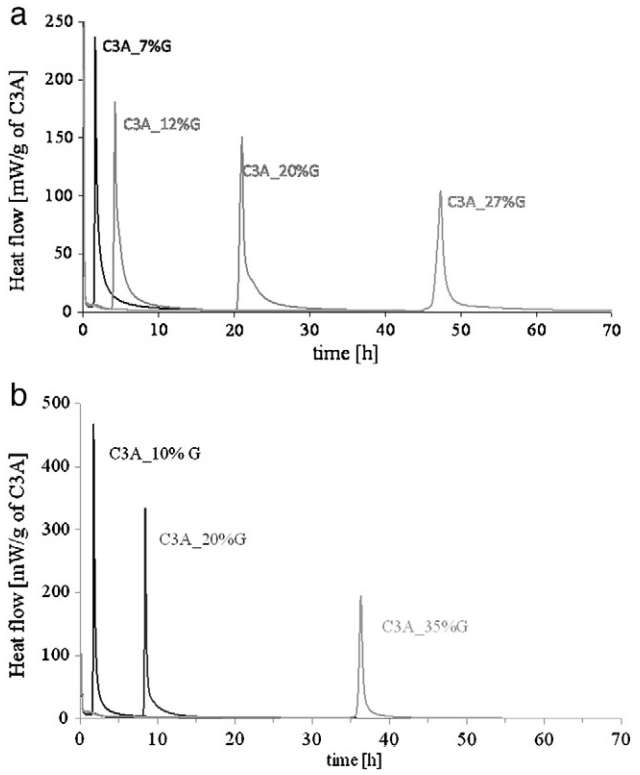

Fig. 3. Examples of heat evolution curves obtained by isothermal calorimetry (20 °C) of C_3A–gypsum systems with different gypsum additions. a) Batch A. b) Batch B. Due to a difference in the PSDs between the different batches differences in the hydration kinetics are observed.

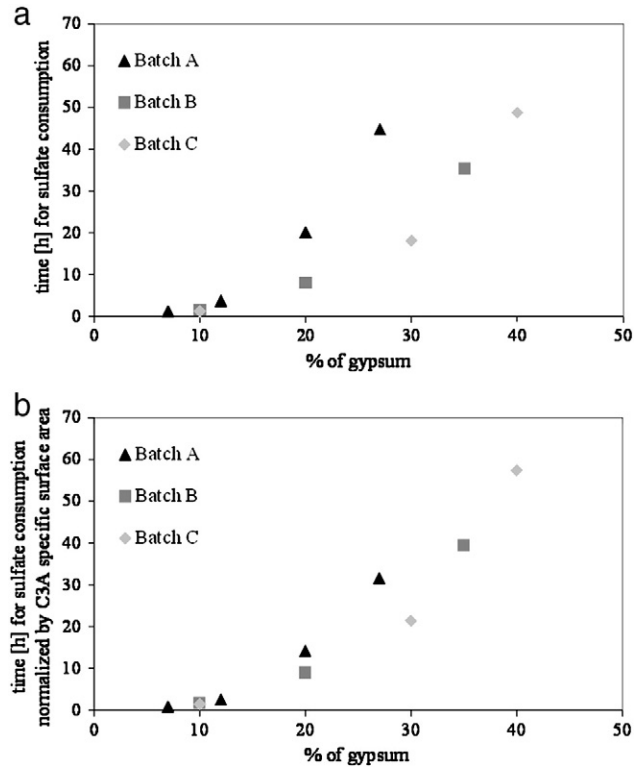

Fig. 4. a) Time necessary for the sulfate consumption as a function of the initial amount of gypsum. The hydration rate depends on the specific surface area of C_3A. A slower rate is observed in the case of Batch A as the C_3A particles are coarser. b) Time necessary for the sulfate consumption as a function of the initial amount of gypsum normalized by the specific surface area of the C_3A. Specific surface areas were estimated based on the particle size distribution measured by laser diffraction and assuming spherical particles.

the beginning of the second stage of the reaction occurs at later ages with increasing gypsum addition.

The first stage of the reaction corresponds to the hydration of C_3A in the presence of gypsum. The hydrate that forms during this period is ettringite. The duration of the first stage of the reaction is longer for systems with higher gypsum content; however the duration of the first stage for a given gypsum addition was not the same for the three batches of C_3A investigated. In Fig. 4a) the time necessary for sulfate consumption has been plotted vs. the initial amount of gypsum, it can be observed that Batches B and C follow the same trend while Batch A reacts at a slower rate, more time is necessary to consume the same amount of gypsum. The main difference between Batches B/C and Batch A is the specific surface area of the C_3A. C_3A from Batches B and C are finer which is reflected in a higher hydration rate. However, if the time necessary for the sulfate consumption is normalized by the initial specific surface area, all the Batches follow a more similar trend as presented in Fig. 4b). This observation is consistent with the findings of Minard et al. [10] who showed the strong influence of particle size distribution on the hydration rate.

The activation energies are reported in Table 2. The relatively high activation energies for this first stage up to the depletion of gypsum (40–80 kJ/mol) are much higher than the value of about 20 kJ/mol which is proposed by Lasaga as differentiating between surface controlled (>20 kJ/mol) and transport controlled (<20 kJ/mol) reactions [15]. These results are coherent with the findings of Minard et al. [10] who suggested that the hydration rate during the first stage of the reaction is controlled by the dissolution of C_3A which is slowed down by the adsorption of sulfate and calcium ions on active sites and not by the formation of a layer of hydrate at C_3A surface. The rate of reaction decreases continually due to the reduction of the surface area of C_3A as the particles dissolve.

3.2. Investigation on the second stage of the reaction (after gypsum depletion)

3.2.1. Evolution of the phase assemblage depending on the gypsum content

The phase assemblage was investigated by in-situ continuous XRD up to 2 days of hydration with the kapton film technique described previously and at defined times at later ages. The hydrates observed for the samples C3A_10G, C3A_20G and C3A_35G (Batch B) are reported in Table 3. After the depletion of gypsum, different phase assemblages were observed depending on the initial gypsum content of the sample. For the samples with high gypsum content (C3A_35G), monosulfoaluminate ($C_4A\$H_{14}$) was the only hydrate present. At later ages, monosulfoaluminate type 12 ($C_4A\$H_{12}$) was observed instead of monosulfo AFm type 14 ($C_4A\$H_{14}$), this is probably due to the fact that less water is present in the system.

In contrast, in the sample with low gypsum content (C3A_10G) only hydroxy-AFm (C_4AH_{19} and /or C_2AH_8) were observed after gypsum consumption (as the X-ray diffraction patterns of C_4AH_{19} and C_2AH_8 are very close, the distinction between the two products could not be

Table 2
Activation energies (Ea) calculated for C_3A–gypsum systems with three different gypsum replacements: 10%, 20% and 35% gypsum (from Batch B). 1st stage of the reaction: in the presence of gypsum. 2nd stage: acceleration after gypsum depletion. Relatively high activation energies (>20 kJ/mol) were obtained. These high Ea are coherent with chemically controlled reactions [15].

	Ea 1st stage (kJ/mol)	Ea 2nd stage (kJ/mol)
C3A_1OG	44 ± 11	21 ± 12
C3A_20G	79 ± 1	59 ± 8
C3A_35G	80 ± 2	44 ± 9

Table 3
Phase assemblage observed by XRD for C_3A–gypsum pastes with three different gypsum replacements: 10%, 20%, 35% (form Batch B).

	Early ages		Later ages		
	In the presence of gypsum	After gypsum depletion	1d	3d	7d
C3A_10G	Ettringite (traces)	C_4AH_{19}/C_2AH_8	$C_4A\$H_{12}$ C_3AH_6 (hemicarboaluminate)	$C_4A\$H_{12}$ C_3AH_6 C_4AH_{19}/C_2AH_8 (traces) (hemicarboaluminate)	$C_4A\$H_{12}$ C_3AH_6 C_4AH_{19}/C_2AH_8 (traces) (hemicarboaluminate)
C3A_20G	Ettringite	$C_4A\$H_{14}$ $C_4A\$H_{12}$ C_4AH_{19}/C_2AH_8	$C_4A\$H_{12}$ C_3AH_6 (hemicarboaluminate)	$C_4A\$H_{12}$ C_3AH_6 C_4AH_{19}/C_2AH_8 (traces) (hemicarboaluminate)	$C_4A\$H_{12}$ C_3AH_6 C_4AH_{19}/C_2AH_8 (traces) (hemicarboaluminate)
C3A_35G	Ettringite	$C_4A\$H_{14}$		$C_4A\$H_{14}$	$C_4A\$H_{14}$ $C_4A\$H_{12}$ (hemicarboaluminate)

made). The sulfate ions present in the systems are probably incorporated in solid solution in the hydroxy-AFm phase. Indeed, many studies, one of the most recent being the work of Matschei [16], have reported formation of solid solutions between hydroxy-AFm and monosulfo-AFm phases. Hydrogarnet peaks were present in the XRD pattern at later ages. The hydrogarnet phase is formed from the metastable hydroxy-AFm phases C_4AH_{19} and C_2AH_8. Some monosulfo-AFm 12 was also observed at later ages. This later formation of monosulfoaluminate can come from the fact that the hydroxy-AFm phases (C_4AH_{19} and/or C_2AH_8) that contain sulfate ions in solid solution have dissolved to form hydrogarnet. As hydrogarnet is not able to incorporate as much sulfate ions as the hydroxy-AFm phases, the sulfate ions become available to form monosulfo-AFm.

The sample C3A_20G shows an intermediate phase assemblage between the C3A_35G and the C3A_10G sample. After gypsum consumption both monosulfo-AFm and very small peaks of hydroxy-AFm (C_4AH_{19} and / or C_2AH_8) were detected. As there is miscibility gap in the solid solution series between monosulfoaluminate and hydroxy-AFm, both phases can co-exist [16]. At later ages hydrogarnet was observed in the sample. For this sample, the water deficient monosulfoaluminate type 12 appears already in the first hours of hydration.

3.2.2. Parameters controlling hydration kinetics during the second stage

With in-situ XRD measurements it is possible to follow the kinetics of the phase evolution during hydration as presented in Fig. 5 for the sample C3A_35G. It was observed that the C_3A and ettringite dissolve rapidly and simultaneously right after gypsum depletion in the paste samples studied here. This is in contrast to the work of Minard et al. [10] in dilute suspensions who found that the dissolution of ettringite does not occur directly after gypsum depletion and that the formation of monosulfoaluminate is a slow process.

Closer examination of the exothermic peaks after sulfate exhaustion reveals that they become lower and broader with increasing gypsum amount in the original mix (Fig. 6). In terms of mechanisms, three possible mechanisms can control the rate of reaction during the acceleration period of the second stage of the reaction. These are considered in turn:

1) the dissolution of ettringite
   If the dissolution of ettringite was the rate controlling mechanism, higher reaction rates should be observed when larger amounts of ettringite are present in the system. However, higher reaction rates were observed for systems with low gypsum content (and therefore small amounts of formed ettringite). Therefore, the dissolution of ettringite cannot be the rate controlling mechanism.
2) the dissolution of C_3A
   If the dissolution of C_3A is the rate controlling mechanism one could expect to observe a sharp increase and then fairly constant rate, but closer examination of the exothermic peaks that occur after sulfate exhaustion on the calorimetric curves obtained in this study reveals that they have more the characteristic shape linked to an acceleration and then a deceleration of the reaction rate than a very sharp shape characteristic of a dissolution.
3) the nucleation and growth of AFm phases
   The heat evolution profiles are characterized by a period in which the reaction accelerates to a peak and then decelerates, especially for the systems with higher gypsum content (Fig. 6). This pattern is coherent with a nucleation and growth mechanism similar to that observed in the alite reaction e.g. [17]. In the Avrami approach, nucleation and growth is a demand based process where the rate of the reaction is not limited by the availability of the reactants. Nuclei grow at a rate proportional to their free surface area leading first to an acceleration. When the individual nuclei

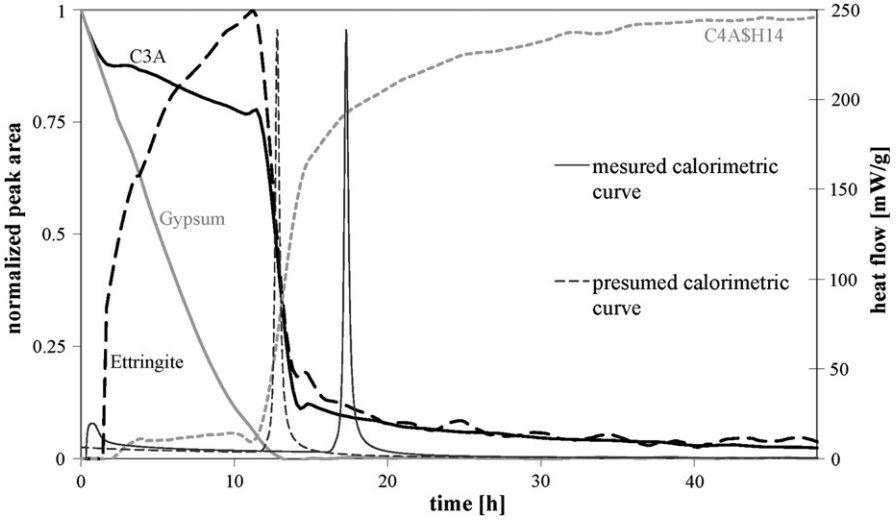

Fig. 5. Evolution of the phase assemblage monitored by in-situ XRD and compared to the calorimetry curve for the sample C3A_35G from Batch B. A rapid dissolution of the C_3A and ettringite to form monosulfoaluminate occurs right after the depletion of gypsum. The difference between this reaction and the exothermic peak measured by calorimetry is probably due to changes in temperature in sample in the XRD chamber during the measurement.

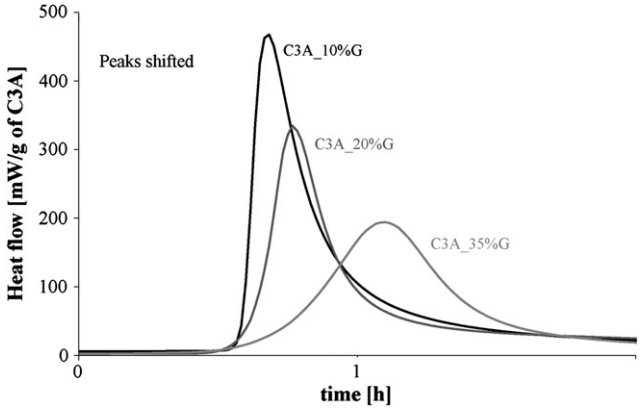

Fig. 6. Close up of the main exothermic peaks of Fig. 3b. The peaks are shifted to be better compared. With increasing gypsum content a significant broadening of the peaks was observed.

start to impinge there is a deceleration due to reduction in the available surface area. The Avrami approach considers homogeneous nucleation, but heterogeneous nucleation follows the same general pattern, as analyzed for example by Cahn [18] or in a numerical simulation by Bishnoi for alite hydration [17]. Here it is hypothesized that heterogeneous nucleation of AFm phases occurs on the C_3A particles at a rate proportional to the available surface area.

Different reaction rates were observed according to the original gypsum content of the system. It has to be considered that with increasing gypsum content two parameters that may influence the rate of the reaction during the acceleration period are modified:

1) The specific surface area of the C_3A remaining when gypsum is exhausted: for higher gypsum additions the second stage of the reaction starts at higher degree of reaction of C_3A, therefore the specific surface area of the particles is smaller. Less C_3A surface available for the nucleation of AFm phases would lead to a lower reaction rate.
2) The space available for the reaction: this decreases because more ettringite is formed during the first stage of the reaction for higher initial gypsum contents as shown in Fig. 7.

The influence of these two parameters on the reaction rate was investigated. The role of the specific surface area on the reaction rate was investigated using C_3A powder sieved in two different and narrow PSDs one called coarse and one fine C_3A (Fig. 1). The heat

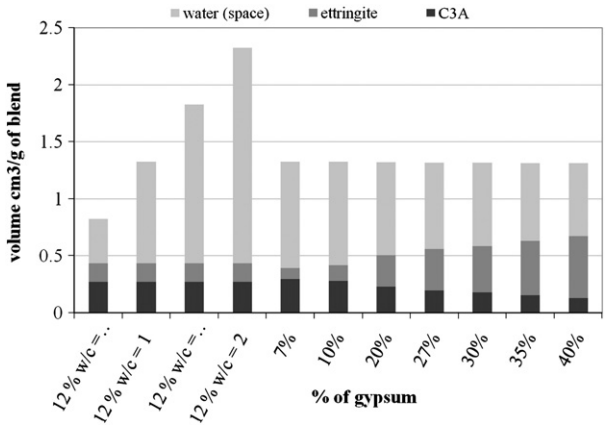

Fig. 7. Theoretical percentage volume available for the reaction at the beginning of the second stage of the reaction for the different samples prepared for this study. Less space is available for the reaction during the second stage of the reaction for higher gypsum additions. These volumes were calculated from stoichiometry assuming that only ettringite is formed during the first stage of the reaction.

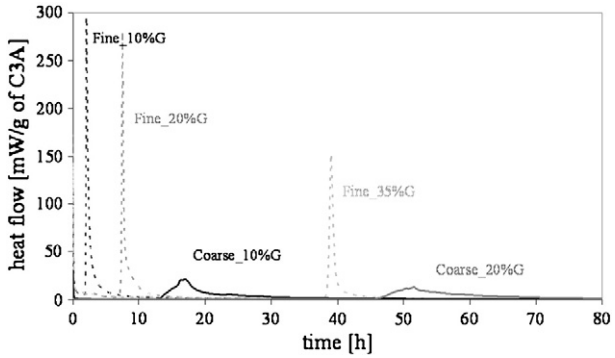

Fig. 8. Heat evolution curves of C_3A–gypsum systems composed of fine and coarse C_3A powders with different gypsum replacements. The exothermic peaks corresponding to the hydration of coarse C_3A particles occur at later ages and are broader.

evolution curves obtained for these fine and coarse systems with different gypsum additions are shown in Fig. 8. The exothermic peaks for the coarser particles are significantly lower and broader for the same gypsum addition. (They also occur later, as the first stage of the reaction is longer due to the lower surface area for C_3A dissolution). The slopes of the exothermic peaks during the acceleration period of the coarser C_3A powder are significantly lower than the slopes of the powder composed of fine particles. The slopes of the exothermic peaks calculated for the finer section of particles are about 1000 times higher than the slope calculated for the coarser ones. The same factor 1000 can be observed between the specific surface area of the fine and coarse particles (surface area calculated from the Dv 50 of the PSD and assuming spherical particles). These results show the strong influence of the specific surface area of C_3A on the acceleration part of the peak. However, is has to be noted that the total peak

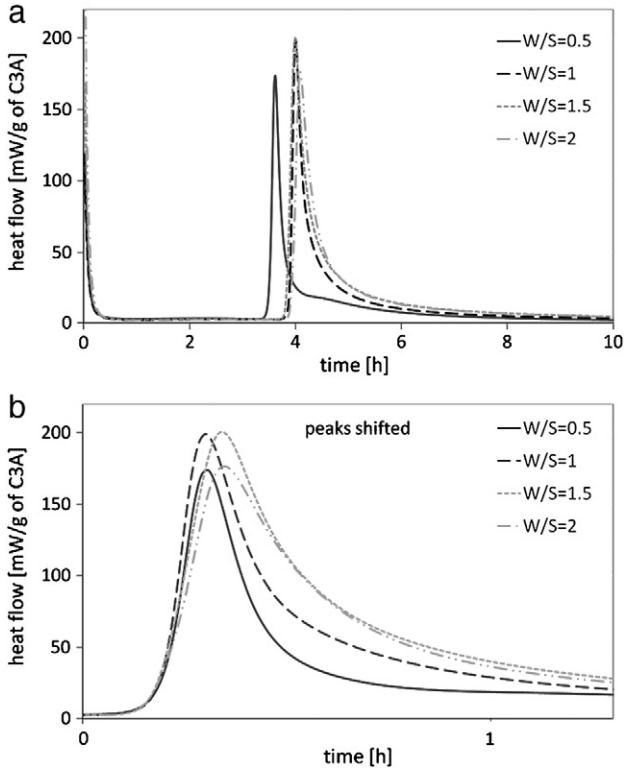

Fig. 9. a) Influence of the water/solid ratio on the shape of the exothermic peak of a C3A_12%G system. b) Close up of the main exothermic peaks of a). The peaks are shifted to facilitate comparison. With a variation of w/s ratio between 0.5 and 2 the deceleration period is strongly affected; a slower deceleration of the reaction is observed for systems where more space is available for the reaction (higher w/s ratios).

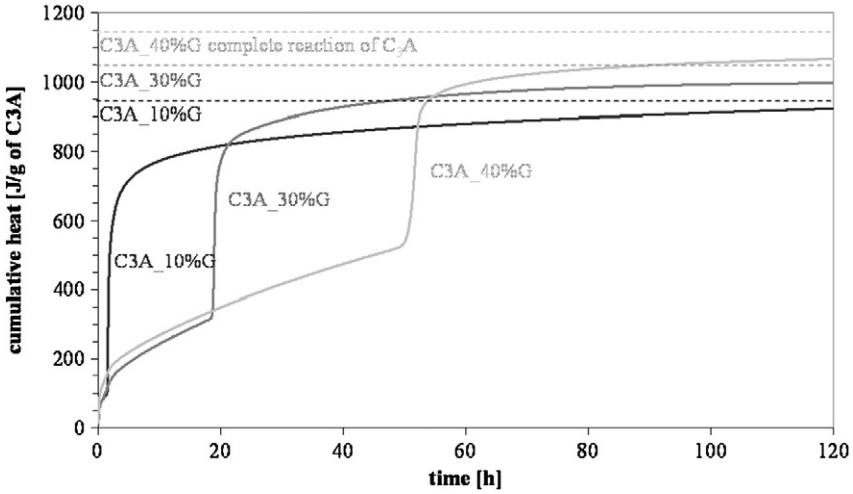

Fig. 10. Cumulative heat curves for the C_3A–gypsum pastes from Batch C. At the end of the exothermic peak the heat released is well below the theoretical heat release for the total reaction of C_3A indicated by a dotted line for the three systems.

area is very similar for the fine and coarse particles. It indicates that the same amount of reaction occurs in both systems, only the kinetics are affected by the size of the C_3A particles.

In order to investigate the influence of the space available for the reaction on the acceleration period, the heat evolution curves of samples composed of 88% C_3A and 12% gypsum with different w/s ratios were monitored. W/s ratios from 0.5 to 2 were investigated as presented in Fig. 9a). The calorimetric peaks were shifted in order to better compare the acceleration periods (Fig. 9b)). No significant differences in the acceleration period were observed when the space available for the reaction is modified by the w/s ratio. The small variations in the acceleration part can be considered to be mainly experimental variations. Increasing the amount of space available should also extend the time for the crystals to impinge, but given that monosulfate crystals have a plate like morphology; growth is favored at the ends of the crystals and an increase in the water to solid ratio will not have so much impact of the grain spacing and so the distance the crystals have to grow before they impinge.

However, the water to solid ratio has a strong impact on the deceleration part of the curve, there is a much more gradual slow down for higher w/s ratios where more space is available. This last observation is coherent with our hypothesis of a reaction rate controlled by the nucleation and growth of AFm hydrates during the acceleration period as the reaction rate decreases when the hydrates start to impinge. For systems where more space is available, the deceleration occurs at a slower rate as there is more space between the crystals after impingement. It can be noted that a similar effect of w/s ratio on deceleration was observed by Gosselin and Scrivener [19] for calcium aluminate cement pastes.

A slowdown in reaction due to lack of reactants may be ruled out. Indeed considerable C_3A unreacted after 1 day can be observed in the micrographs and the heat released for a complete reaction is not archived at the end of the exothermic peak, as shown in Fig. 10. The heat released for a complete reaction of C_3A was calculated for each sample with the following method: first the amount of C_3A involved in ettringite, monosulfoaluminate and hydrogarnet formation was calculated from stoichiometry. Then the theoretical total heat was calculated by addition of the heat released for ettringite (1670 J/g of C_3A [20]), monosulfoaluminate (881 J/g) and hydrogarnet (907 J/g) formation weighted by the contribution of each reaction. For example for the sample C3A_30G: 22.4% of the C_3A is used in ettringite formation, 44.8% in monosulfoaluminate formation and 32.8% remain and form hydrogarnet at later ages. Therefore the total heat is $0.224 \times 1670\ J/g + 0.448 \times 881\ J/g + 0.328 \times 907\ J/g = 1066\ J/g$. At the end of the exothermic peak, the total heat released is well below this value indicating that enough C_3A is still present in the system. In addition, a water to solids ratio of 1 is in excess of that needed stoichiometrically (although it cannot be ruled out that this may be a factor in the mixture made at 0.5).

These two experiments suggest that the surface area of the C_3A, where AFm phases nucleate is the main factor controlling the acceleration period and that the space available for the growth controls the deceleration part. In the series of samples with increasing gypsum (Fig. 6) these factors interact in a quite complex way. Indeed, for the samples with high gypsum content, where there is more reaction in the first stage, there is less surface area available for reaction at the second stage and a lower slope in the acceleration period is observed.

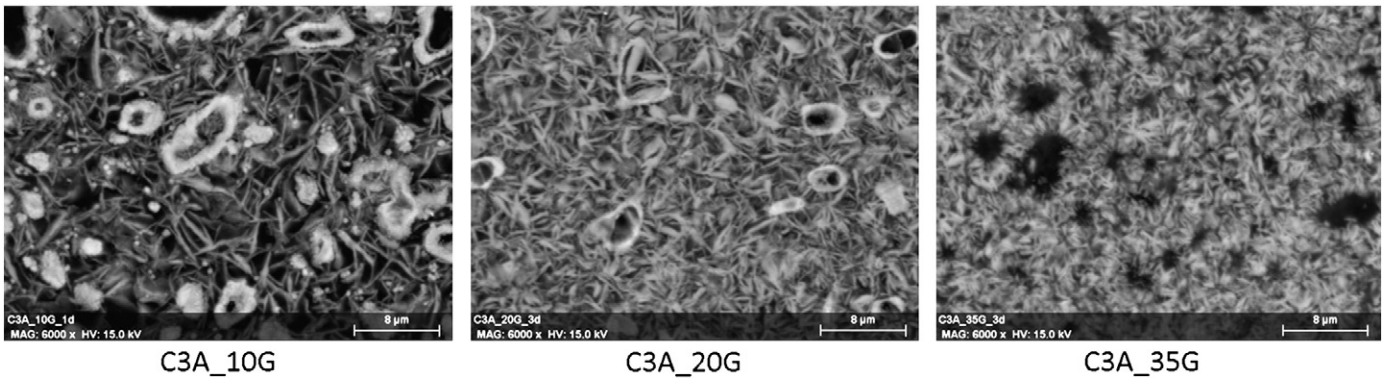

Fig. 11. Morphology of the AFm platelets depending on the gypsum content. The AFm platelets are shorter for the pastes with higher original gypsum content.

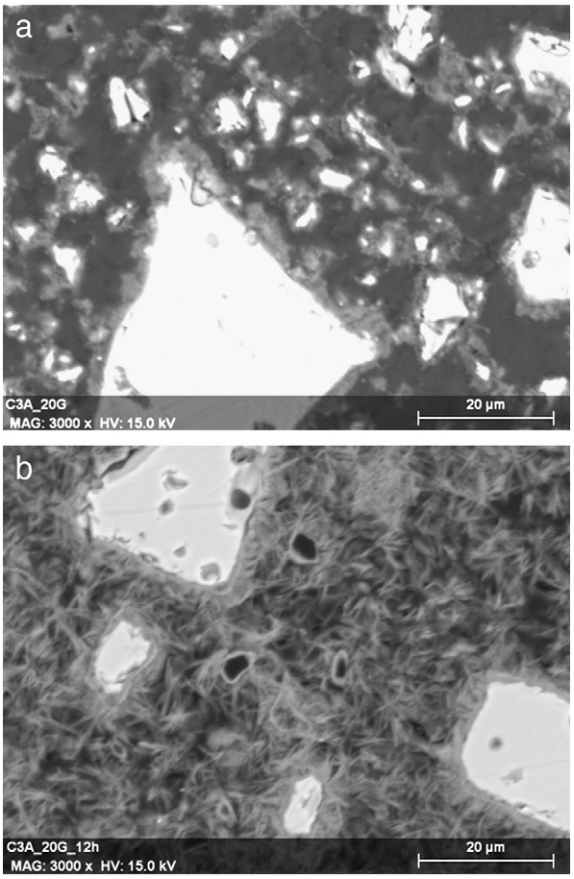

Fig. 12. Microstructures of a C_3A–20% gypsum paste before (a) and after (b) gypsum depletion. A significant densification that corresponds to the formation of monosulfoaluminate can be observed between these two images.

The lower amount of space leads to the formation of smaller plates of AFm as reflected in the microstructure at 1 day, Fig. 11.

It is noted that higher additions of gypsum do not seem to have the same effect on the height and shape of the peaks for this second stage in the experiments of Minard et al. [10] carried out in suspension. However many factors change between pastes and suspensions; it was already noted that we see the rapid formation of AFm phase immediately after the exhaustion of gypsum whereas there was a delay in the case of suspensions studied by Minard et al. This suggests that the dissolution of C_3A may play a more significant role in this latter case, as may the exhaustion of C_3A as there is considerable space available in solution.

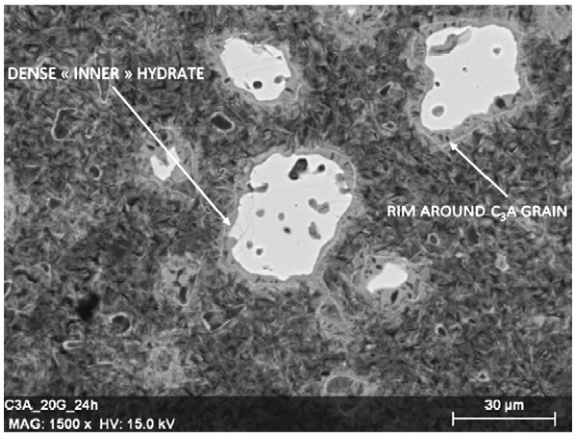

Fig. 13. Microstructures of a C_3A–20% gypsum paste at 24 h of hydration. AFm phases form as platelets in the space between the grains and as a dense hydrate that grows within the grain boundaries. Hydrogarnet was observed forming a rim around the hydrating C_3A grains.

In addition to the analysis of the calorimetric curves, the activation energies of these reactions were calculated from the calorimetric curves measured at different temperatures. The high activation energies obtained for the second stage of the reaction for all the gypsum additions (reported in Table 2) remained constant throughout this second stage and the high values are again coherent with a surface controlled mechanism (e.g., nucleation and growth of AFm phases). Similar activation energies were obtained for the samples C3A_20G and C3A_35G samples for both first and second stages of the reaction. Lower Ea were obtained for the sample C_3A_10G, but there is a much greater potential error for the low gypsum addition as the first stage of the reaction is very short, especially at high temperature and the measurement may be influenced by the introduction of the sample in the calorimeter. Therefore the temperature may be not perfectly stable during the first minutes of reaction and the calculation of Ea may have been influenced.

3.2.3. Microstructural development during and after the second reaction peak

The in-situ XRD results show that the reaction of C_3A and ettringite to form monosulfoaluminate (and/or hydroxy-AFm) after gypsum depletion occurs rapidly. The microstructures observed by SEM show a rapid and significant densification of the matrix right after gypsum depletion with the precipitation of AFm platelets (Fig. 12). As hydration proceeds, rims of "inner" hydrate with a monolithic appearance and no apparent porosity form around the grains. These regions seem to develop within the original grain boundaries (Fig. 13). EDS microanalysis of this "inner hydrate" showed that it has a similar composition but with a slightly lower sulfate content to the hydrate present in the matrix (Fig. 14). The difference in composition can probably be attributed to the proximity of the C_3A grains, which may be included in the interaction volume of the analyses. This "inner" hydrate was less obvious at later ages. Possible reasons for this may be re-crystallization as matrix product and/or hydrogarnet. The chemical composition of both matrix and "inner" hydrate measured by EDS analysis suggests the formation of a solid solution between $C_4A\$H_{14}$ and the hydroxy-AFm phases C_4AH_{19} and C_2AH_8. However, as there is miscibility gap in the solid solution series between monosulfoaluminate and hydroxy-AFm [16] and both phases were observed by XRD the sample with 20% of gypsum addition, the existence of a fine mixture of these phases at a sub-micron scale cannot be ruled out, even though in this latter case a more dispersed cloud of points would have been expected. Although the EDS points are scattered on the line joining $C_4A\$H_{14}$ and C_3AH_6, a mixture of these two phases is unlikely especially in the case of the "inner" hydrate that has a monolithic appearance. Moreover, C_3AH_6 was clearly observed in the microstructure from 24 h forming a thin

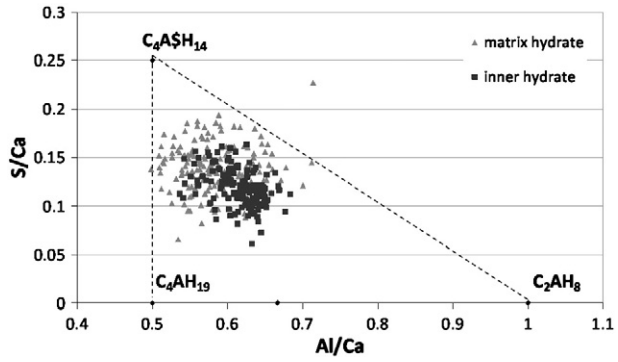

Fig. 14. EDS analysis of the hydrates at 24 h of hydration for the sample C_3A–20% gypsum. The chemical composition of both matrix and "inner" hydrate is between $C_4A\$H_{14}$ and the hydroxyl-AFm phases C_4AH_{19} and C_2AH_8.

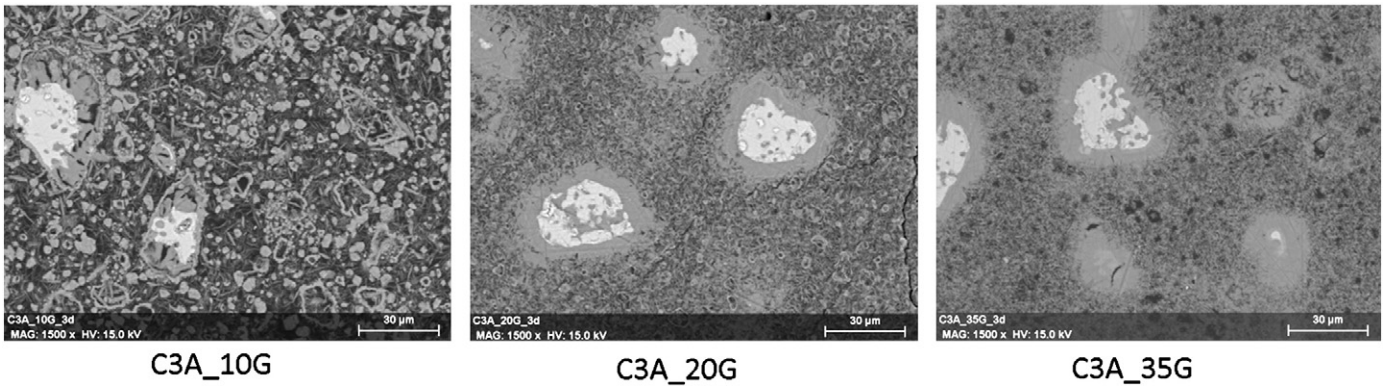

Fig. 15. Microstructures of C_3A–gypsum pastes with three gypsum replacements: 10%, 20%, 35%. AFm platelets and "inner" product can be observed in all the microstructure. Hydrogarnet shells were present only for the lowers gypsum additions.

rim around the "inner" hydrate for the two lower levels of gypsum addition (Fig. 13). It is proposed that the hydrogarnet layer is located at the original C_3A grain boundaries. Indeed, at the very beginning of the reaction several authors have reported the formation of hydroxy-AFm phases on the C_3A surface, as previously discussed [3–8,10,12]. As these AFm phases are metastable, they may have converted at later ages to hydrogarnet remaining where they originally formed. When the C_3A grains are completely hydrated, hollow hydrogarnet shells can be observed in the microstructure.

3.2.4. Influence of the initial gypsum content on the microstructure

Quite a similar microstructural development was observed for the samples with intermediate and high gypsum content (Fig. 15) except that no hydrogarnet shell was present in the microstructure for the C3A_35G sample, even at later ages. Only the "inner" product or empty grains surrounded by monosulfoaluminate were observed. However, there is some variation in the chemical composition and the morphology of the hydrates. The composition of the matrix hydrate was observed to be very close to the stoichiometric composition of monosulfoaluminate for the sample with high gypsum content (Fig. 16). The morphology of the hydrates is also different. The AFm platelets of the matrix hydrate are shorter than the platelets observed for the samples with intermediate gypsum content, as discussed above in the analysis of mechanisms controlling kinetics (Fig. 11). At the lowest gypsum content the microstructure was significantly different to the other two systems. The three hydrates observed for the others gypsum replacements (matrix hydrate, inner product and hydrogarnet shell) are also present but in different amounts. The paste is mainly composed of thick hydrogarnet shells with long thin

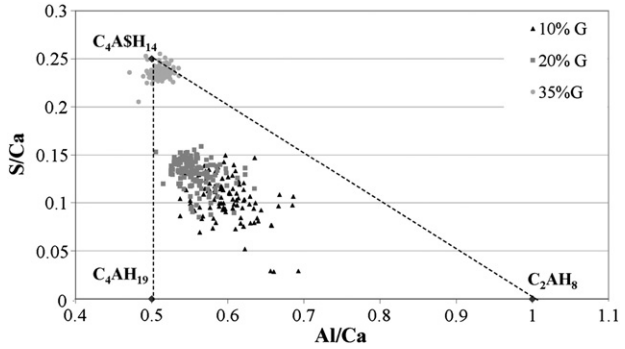

Fig. 16. EDS analysis of the hydrates for C_3A–gypsum pastes with three different gypsum replacements: 10%, 20% and 35%. Different compositions in the solid solution series between $C_4A\$H_{14}$ and the hydroxyl-AFm phases C_4AH_{19} and C_2AH_8 form depending on the initial gypsum addition.

AFm crystals in the matrix, which are probably a solid solution of hydroxy-AFm phases with sulfate incorporated.

4. Conclusions

The results we obtained for the first stage of the reaction of C_3A and gypsum show a strong influence of the specific surface area of C_3A on the hydration rate. This observation as well as the high activation energies calculated for all the systems is coherent with the rate controlling mechanism being the dissolution of C_3A controlled by the absorption of sulfate ions, in agreement with the conclusions of Minard et al. [10].

New results were obtained on the second stage of the reaction, when gypsum is depleted.

- It was shown that the dissolution of C_3A and ettringite to form monosulfoaluminate, in pastes, is a rapid reaction that takes place right after the depletion of gypsum.
- This reaction is characterized by a sharp exothermic peak in the heat evolution. The acceleration of the reaction rate was shown to be highly influenced by the remaining surface area of the reacting C_3A particles and the rate controlling mechanism is hypothesized to be the nucleation and growth of AFm phases on the C_3A surfaces. The deceleration part of the peak seems to depend on the space available, consistent with the reaction being limited by the impingement of AFm crystals.

The microstructural study shows the presence of an inner hydrate that grows within the C_3A grain boundaries. The evolution of the morphology over time suggests the rapid formation of small and maybe poorly crystalline material which later recrystallizes as coarser crystals. Rims of hydrogarnet form at the location of the original surface of the C_3A grains, probably from the first formation of hydroxy-AFm phases.

Acknowledgments

The Swiss National Science Foundation is acknowledged for the financial support. The authors would like to thank Cyrille F. Dunant for his precious help with the XRD data processing and Gaurav Sant for helpful discussions on the calculation of the activation energies. We would like to thank also Emmanuel Gallucci for all his helpful comments and Aditya Kumar for discussion throughout the study.

References

[1] M. Collepardi, G. Baldini, M. Pauri, M. Corradi, Tricalcium aluminate hydration in the presence of lime, gypsum or sodium sulfate, Cem. Concr. Res. 8 (1978) 571–580.

[2] H.N. Stein, J.M. Stevels, Influence of silica on the hydration of $3CaO,SiO_2$, J. Appl. Chem. 14 (1964) 338–346.
[3] P.W. Brown, L.O. Liberman, G. Frohnsdorff, Kinetics of the early hydration of tricalcium aluminate in solution containing calcium sulfate, J. Am. Ceram. Soc. 67 (1984) 793–795.
[4] W.A. Corstanje, H.N. Stein, J.M. Stevels, Hydration reactions in pastes $C_3S + C_3A + CaSO_4.2aq + H_2O$ at 25°C.I, Cem. Concr. Res. 3 (1973) 791–806.
[5] W.A. Corstanje, H.N. Stein, J.M. Stevels, Hydration reactions in pastes $C_3S + C_3A + CaSO_4.2aq +$ water at 25°C. II, Cem. Concr. Res. 4 (1974) 193–202.
[6] W.A. Corstanje, W.N. Stein, J.M. Stevels, Hydration reactions in pastes $C_3S + C_3A + CaSO_4.2aq. +$ water at 25°C.III, Cem. Concr. Res. 4 (1974) 417–431.
[7] P.S. Gupta, S. Chatterji, W. Jeffrey, Studies of the effect of different additives on the hydration of tricalcium aluminate: part 5—a mechanism of retardation of C_3A hydration, Cem. Technol. 4 (1973) 146–149.
[8] K.L. Scrivener, P.L. Pratt, Microstructural studies of the hydration of C_3A and C_4AF independently and in cement paste, Proc. Br. Ceram. Soc 35 (1984) 207–219.
[9] R.F. Feldman, V.S. Ramachandran, The influence of $CaSO_4.2H_2O$ upon the hydration character of $3CaO.Al_2O_3$, Mag. Concr. Res. 18 (1966) 185–196.
[10] H. Minard, S. Garrault, L. Regnaud, A. Nonat, Mechanisms and parameters controlling the tricalcium aluminate reactivity in the presence of gypsum, Cem. Concr. Res. 37 (2007) 1418–1426.
[11] J. Skalny, M.E. Tadros, Retardation of tricalcium aluminate hydration by sulfates, J. Am. Ceram. Soc. 60 (1977) 174–175.
[12] S. Pourchet, L. Regnaud, J.P. Perez, A. Nonat, Early 432 C_3A hydration in the presence of different kinds of calcium sulfate, Cem. Concr. Res. 39 (2009) 989–996.
[13] N.J. Carino, Handbook on Nondestructive Testing of Concrete: Second Edition, Chapter 5: The Maturity Method, CRC Press, 2006.
[14] G. Le Saoût, T. Fullmann, V. Kocaba, K. Scrivener, Quantitative study of cementitious materials by X-ray diffraction/Rietveld analysis using external standard, Proceedings of the 12th International Congress of the Chemistry of Cement, Montreal, Canada, 2007.
[15] A.C. Lasaga, Kinetic Theory in the Earth Sciences ed. P.s.i. Geochemistry, Princeton University Press, 1998.
[16] T. Matschei, B. Lothenbach, F.P. Glasser, The AFm phase in Portland cement, Cem. Concr. Res. 37 (2007) 118–130.
[17] S. Bishnoi, K.L. Scrivener, Studying nucleation and growth kinetics of alite hydration using μic, Cem. Concr. Res. 39 (2009) 849–860.
[18] J.W. Cahn, The kinetics of grain boundary nucleation reactions, Acta Metall. 4 (1956) 449–559.
[19] C. Gosselin, E. Gallucci, K. Scrivener, Influence of self heating and Li2SO4 addition on the microstructural development of calcium aluminate cement, Cem. Concr. Res. 40 (2010) 1555–1570.
[20] H.F.W. Taylor, Cement Chemistry, in: Thomas Telford (Ed.), 2nd edition, 1997.